

1  
2  
3  
4  
5  
6  
7  
8  
9  
10  
11

**Revision 2**

**Goldschmidtite, (K,REE,Sr)(Nb,Cr)O<sub>3</sub>: a new perovskite supergroup mineral  
found in diamond from Koffiefontein, South Africa**

Nicole A. Meyer\*<sup>1</sup>, Michelle D. Wenz<sup>2</sup>, James P. S. Walsh<sup>3</sup>, Steven D. Jacobsen<sup>2</sup>,  
Andrew J. Locock<sup>1</sup>, and Jeffrey W. Harris<sup>4</sup>

\*corresponding author email: [nameyer@ualberta.ca](mailto:nameyer@ualberta.ca)

12   <sup>1</sup>Department of Earth and Atmospheric Sciences  
13   1-26 Earth Sciences Building  
14   University of Alberta  
15   Edmonton, Alberta, Canada, T6G 2E3  
16  
17   <sup>2</sup>Department of Earth and Planetary Sciences  
18   Northwestern University  
19   2145 Sheridan Road  
20   Technological Institute  
21   Evanston, Illinois, USA, 60208  
22  
23   <sup>3</sup>Department of Chemistry  
24   Northwestern University  
25   2145 Sheridan Road  
26   Evanston, Illinois, USA, 60208  
27  
28   <sup>4</sup>School of Geographical and Earth Sciences  
29   University of Glasgow  
30   The Gregory Building  
31   Lilybank Gardens  
32   Glasgow, Scotland, United Kingdom, G12 8QQ  
33  
34

35 **ABSTRACT**

36 Goldschmidtite is a new perovskite-group mineral (IMA No. 2018-034) with ideal formula  
37 (K,REE,Sr)(Nb,Cr)O<sub>3</sub>. A single grain of goldschmidtite with maximum dimension of ~100 μm  
38 was found as an inclusion in a diamond from the Koffiefontein pipe in South Africa. In addition  
39 to the dark green and opaque goldschmidtite, the diamond contained a Cr-rich augite (websteritic  
40 paragenesis) and an intergrowth of chromite, Mg-silicate, and unidentified K-Sr-REE-Nb-oxide.  
41 Geothermobarometry of the augite indicates the depth of formation was ~170 km. The chemical  
42 composition of goldschmidtite determined by electron microprobe analysis (n = 11, WDS, wt%)  
43 is: Nb<sub>2</sub>O<sub>5</sub> 44.82, TiO<sub>2</sub> 0.44, ThO<sub>2</sub> 0.10, Al<sub>2</sub>O<sub>3</sub> 0.35, Cr<sub>2</sub>O<sub>3</sub> 7.07, La<sub>2</sub>O<sub>3</sub> 11.85, Ce<sub>2</sub>O<sub>3</sub> 6.18, Fe<sub>2</sub>O<sub>3</sub>  
44 1.96 MgO 0.70, CaO 0.04, SrO 6.67, BaO 6.82, K<sub>2</sub>O 11.53, total 98.53. The empirical formula  
45 (expressed to two decimal places) is  
46 (K<sub>0.50</sub>La<sub>0.15</sub>Sr<sub>0.13</sub>Ba<sub>0.09</sub>Ce<sub>0.08</sub>)<sub>Σ0.95</sub>(Nb<sub>0.70</sub>Cr<sub>0.19</sub>Fe<sub>0.05</sub>Al<sub>0.01</sub>Mg<sub>0.04</sub>Ti<sub>0.01</sub>)<sub>Σ1.00</sub>O<sub>3</sub>. Goldschmidtite is  
47 cubic, space group *Pm-3m*, with unit-cell parameters:  $a = 3.9876(1) \text{ \AA}$ ,  $V = 63.404(6) \text{ \AA}^3$ ,  $Z = 1$ ,  
48 resulting in a calculated density of 5.32(3) g/cm<sup>3</sup>. Goldschmidtite is the K-analogue of  
49 isolueshite, (Na,La)NbO<sub>3</sub>. Raman spectra of goldschmidtite exhibit many second-order broad  
50 bands at 100 to 700 cm<sup>-1</sup> as well as a pronounced peak at 815 cm<sup>-1</sup>, which is possibly a result of  
51 local ordering of Nb and Cr at the B site. The name goldschmidtite is in honor of the eminent  
52 geochemist Victor Moritz Goldschmidt (1888 – 1947), who formalized perovskite crystal  
53 chemistry and identified KNbO<sub>3</sub> as a perovskite-structured compound.

54  
55 **Keywords:** perovskite, niobium, mantle, diamond inclusion, new mineral, Koffiefontein,  
56 Kaapvaal

57

58

## INTRODUCTION

59       Diamonds are carriers of minerals from the lithospheric mantle underpinning cratons (Harris  
60 and Gurney 1979; Meyer 1987; Helmstaedt et al. 2010), the mantle transition zone (Pearson et al.  
61 2014; Kiseeva et al. 2015; Tschauner et al. 2018), and the lower mantle (Harte et al. 1999;  
62 Tschauner et al. 2014; Palot et al. 2016; Nestola et al. 2018). As a chemically inert and rigid  
63 host, diamond can preserve included minerals for billions of years, and thus provide a snapshot  
64 of ancient chemical conditions in cratonic keels or deep-mantle regions.

65       The Kaapvaal craton in South Africa is host to many diamondiferous kimberlites that have  
66 been intensively mined and studied since the 1970s (e.g., the International Kimberlite  
67 Conferences held since 1973). Large-scale mining, large inclusion-bearing diamonds, and the  
68 efforts of geochemists globally, have made it the most-studied craton from the perspective of  
69 diamond formation.

70       We report the first natural occurrence of  $(\text{K,REE,Sr})(\text{Nb,Cr})\text{O}_3$ , now named goldschmidtite  
71 (IMA No. 2018-034), included in a websteritic diamond from the Koffiefontein kimberlite,  
72 Kaapvaal craton, South Africa. The holotype specimen is deposited in the Royal Ontario  
73 Museum, accession number M58208. It is the fifth perovskite-structured mineral to occur in  
74 Earth's mantle, along with perovskite *sensu stricto* ( $\text{CaTiO}_3$ ), bridgmanite (Harte et al. 1999;  
75 Tschauner et al. 2014),  $\text{CaSiO}_3$ -perovskite (Nestola et al. 2018), and K-REE-Cr-rich tausonite,  
76 which previously recorded the highest Nb- and K-content in a perovskite mineral-inclusion from  
77 diamond (Kopylova et al., 1997).

78       Goldschmidtite is the natural analogue of the well-known ferroelectric material  $\text{KNbO}_3$ ,  
79 which has the perovskite structure type with orthorhombic symmetry at room temperature  
80 (coexisting with a metastable monoclinic phase: Lummen et al. 2017), and whose symmetry

81 increases to cubic above  $\sim 400$  °C (Skjærvø et al. 2018). Solid solution of  $\text{LaFeO}_3$  in  $\text{KNbO}_3$ , at  
82 molar amounts of 20% or more, also has the effect of increasing the symmetry to cubic at room  
83 temperature (Kakimoto et al. 2003).

84 End-member  $\text{KNbO}_3$  was first synthesized by Joly (1877), as discussed by Holmquist (1896).  
85 Thomas F.W. Barth, a member of Victor Moritz Goldschmidt's research group, was the first to  
86 determine the crystal structure of perovskite,  $\text{CaTiO}_3$  (Barth 1925). In the following year,  
87 Goldschmidt and his group reported that  $\text{KNbO}_3$  was effectively isostructural, and  
88 simultaneously introduced the famous tolerance factor for prediction of the perovskite structure  
89 type (Goldschmidt 1926).

90 Goldschmidtite is named in honor of the eminent scientist Victor Moritz Goldschmidt (born  
91 Zürich, 27 January 1888; died Oslo, 20 March 1947). Goldschmidt made very wide-reaching  
92 contributions in geology, chemistry, mineralogy, crystallography, and petrology (Tilley 1948;  
93 Bastiansen 1962; Suess 1988; Mason 1992; Kauffman 1997). He is widely recognized as the  
94 “founder of modern geochemistry” (Bastiansen 1962; Kauffman 1997), and as stated by Laves  
95 (1962): “The influences of V. M. Goldschmidt's work on the development of mineralogy and  
96 crystallography cannot be overestimated.”

97 The name goldschmidtite was briefly used (Hobbs 1899) for a supposed gold-silver telluride,  
98  $\text{Au}_2\text{AgTe}_6$ , that was shown later to be sylvanite (Palache 1900). Similarly, goldschmidtine was  
99 used (Peacock 1939) for a supposed antimonide of silver,  $\text{Ag}_2\text{Sb}$ , that was shown subsequently to  
100 be stephanite (Peacock 1940). Both of these names had been intended to honor the celebrated  
101 crystallographer Victor Mordechai Goldschmidt (born 10 February 10, 1853; died 8 May 1933).

102 Following the recently revised nomenclature for minerals of the perovskite supergroup  
103 (Mitchell et al. 2017), goldschmidtite is a member of the perovskite subgroup and is the  
104 potassium-analogue of isolueshite, (Na,La)NbO<sub>3</sub> (Chakhmouradian et al. 1997).

105

106

#### OCCURRENCE

107 The 90.4 Ma Koffiefontein kimberlite pipe is located about 80 km SSE of Kimberley, South  
108 Africa and was emplaced in the Archean basement of the Kaapvaal craton and overlying  
109 Phanerozoic sediments of the Karoo basin (Davis 1978; Clement 1982; Naidoo et al. 2004; Field  
110 et al. 2008). This diamondiferous kimberlite was discovered in 1870 (Field et al. 2008) and has  
111 been mined for diamonds intermittently.

112 The diamonds from Koffiefontein are dominantly peridotitic (determined from silicate  
113 inclusions: Harris and Gurney, 1979; Rickard et al. 1989). Goldschmidtite was found in a  
114 websteritic assemblage in association, but not in direct contact, with Cr-rich augite, and an  
115 intergrowth of chromite, Mg-silicate, and an unidentified K-Sr-REE-Nb-oxide. In this region of  
116 the diamond surface there was both green and brown radiation damage (Figure 1). The Cr-  
117 content (1.19 wt% Cr<sub>2</sub>O<sub>3</sub>) and Mg# (86) of the included augite suggests that the host diamond  
118 formed in websterite (Gurney et al. 1984). From single-clinopyroxene geothermobarometry  
119 (Nimis and Taylor 2000), an equilibration pressure of 53 kbar (about 170 km depth) and  
120 temperature of formation of 1190 °C can be calculated.

121

122

## EXPERIMENTAL DETAILS

123

The goldschmidtite inclusion was released from its host diamond by mechanical

124

fracturing of the diamond with a steel diamond cracker. The released mineral was mounted in

125

epoxy, roughly ground with corundum paper, and polished with 1  $\mu\text{m}$  diamond suspension on a

126

nylon cloth.

127

A Cameca SX100 electron microprobe at the University of Alberta was used to examine a

128

polished and carbon-coated (25 nm thickness) epoxy mount of goldschmidtite. In addition to

129

secondary-electron and back-scattered electron images, quantitative spot analyses were acquired

130

using wavelength-dispersive spectrometry and Probe for EPMA software (Donovan et al. 2015).

131

Nineteen elements were measured (Na, Mg, Al, Si, K, Ca, Ti, Cr, Fe, Sr, Zr, Nb, Ba, La, Ce, Nd,

132

Pr, Sm, and Th) with the following conditions: 20 kV accelerating voltage, 30 nA probe current,

133

and  $<1 \mu\text{m}$  beam diameter (5  $\mu\text{m}$  was used for the standards). Total count times of 40 seconds

134

were used for both peaks and backgrounds. The X-ray lines, diffraction crystals, and standards

135

were: Na  $K\alpha$ , TAP (thallium hydrogen phthalate), albite; Mg  $K\alpha$ , TAP, pyrope; Al  $K\alpha$ , TAP,

136

Gore Mountain garnet; Si  $K\alpha$ , TAP, diopside; K  $K\alpha$ , PET (pentaerythritol), sanidine; Ca  $K\alpha$ ,

137

PET, diopside; Ti  $K\alpha$ , PET, SrTiO<sub>3</sub>; Cr  $K\alpha$ , LIF, Cr<sub>2</sub>O<sub>3</sub>; Fe  $K\alpha$ , LIF (lithium fluoride), fayalite;

138

Sr  $L\alpha$ , PET, SrTiO<sub>3</sub>; Zr  $L\alpha$ , PET, zircon; Nb  $L\alpha$ , PET, niobium metal; Ba  $L\gamma$ , PET, sanbornite; La

139

$L\alpha$ , LIF, LaPO<sub>4</sub>; Ce  $L\alpha$ , LIF, CePO<sub>4</sub>; Nd  $L\beta$ , LIF, NdPO<sub>4</sub>; Pr  $L\beta$ , LIF, PrPO<sub>4</sub>; Sm  $L\beta$ , LIF,

140

SmPO<sub>4</sub>; Th  $M\alpha$ , PET, ThO<sub>2</sub>. The X-ray intensity data were reduced following Armstrong (1995)

141

with the mass-absorption coefficients of Chantler et al. (2005). For elements found above the

142

detection limits interference corrections (Donovan et al. 2011) were applied to: Al for

143

interference by Th; Ti for interference by Ba; Cr for interference by La; Fe for interference by

144

Th; Sr for interference by Cr; Ce for interference by Ba; and Th for interference by Cr. The

145 following elements were not found above the limits of detection (as element in weight percent in  
146 parentheses): Na (0.01), Si (0.01), Zr (0.04), Pr (0.08), Nd (0.05), and Sm (0.05).

147 The crystal of goldschmidtite was extracted from the epoxy block and mounted on to a glass  
148 fiber with isocyanocrylate adhesive. High-precision unit-cell parameters were determined by  
149 single-crystal X-ray diffraction by the eight-position centering method (King and Finger 1979)  
150 on the Huber four-circle diffractometer at Northwestern University equipped with an SMC9300  
151 controller and sealed-tube Mo  $K\alpha$  radiation source. A 360° phi-rotation image was collected on a  
152 MAR345 image plate detector. Full-profile peak fitting was performed with the software  
153 package SINGLE (Angel and Finger 2011). In total, 46 reflections were centered using omega  
154 scans (rocking curves) in their eight-equivalent positions with a point detector 40 cm from the  
155 crystal at 2 $\theta$  angles between  $\pm 30^\circ$ . Intensity data used to produce a crystallographic information  
156 file (.cif) were collected from -15 to +60 degrees 2 $\theta$  also using the point detector on the four-  
157 circle diffraction system at Northwestern University.

158 Confocal Raman spectroscopy was carried out at Northwestern University using a custom-  
159 built system with an Olympus BX microscope with a Mitutoyo 100X objective. A Melles-Griot  
160 (Model 85-BLS-601) solid-state, diode-pumped laser with 200 mW output and wavelength of  
161 458.5 nm was used as the excitation source. The output power was reduced with neutral density  
162 filters to achieve an ~8 mW focused beam of ~1-2  $\mu\text{m}$  diameter at the sample surface.  
163 Unpolarized Raman spectra were collected in back-scatter geometry through a confocal aperture  
164 into a 0.5 m focal-length Andor Shamrock 303i spectrograph with 1200 lines-per-mm diffraction  
165 grating. Spectra were collected on an Andor Newton DU970 CCD camera cooled to -90 °C with  
166 a thermoelectric cooler. Spectra were obtained for 10 seconds, averaged over 12 accumulations  
167 for a total of two minutes per spectrum.



168

## RESULTS AND DISCUSSION

### 169 **Physical and properties**

170 Only a single grain of goldschmidtite, about 100  $\mu\text{m}$  in maximum dimension, was  
171 recovered. The mineral is dark green with an adamantine luster, non-fluorescent under longwave  
172 UV illumination, and is not cathodoluminescent. The small size of the solitary mineral grain  
173 precluded determination of its streak and hardness, and the tenacity, fracture, and cleavage were  
174 not observed. From the average chemical composition determined by EPMA and the unit cell  
175 parameters, the calculated density is 5.32(3)  $\text{g}/\text{cm}^3$ . The refractive index was calculated to be:  
176  $n_{\text{calc}} 2.16(2)$ , with the use of the Gladstone-Dale constants of Mandarino (1976), the calculated  
177 density, and the average chemical composition. Stacked optical images of goldschmidtite  
178 acquired with a Tagarno Prestige FHD digital microscope are shown in Figure 2.

179

### 180 **Chemical composition**

181 The average composition of goldschmidtite, for elements above detection, is given in Table  
182 1; the iron content is reported as total  $\text{Fe}_2\text{O}_3$  by analogy with latrappite,  $(\text{Ca},\text{Na})(\text{Nb},\text{Ti},\text{Fe})\text{O}_3$   
183 (Mitchell et al. 1998). The empirical formula, calculated on the basis of three anions, is:  
184  $(\text{K}_{0.504}\text{La}_{0.150}\text{Sr}_{0.133}\text{Ba}_{0.092}\text{Ce}_{0.078}\text{Ca}_{0.002}\text{Th}_{0.001})_{\Sigma 0.960}$   
185  $(\text{Nb}_{0.695}\text{Cr}_{0.192}\text{Fe}_{0.051}\text{Al}_{0.014}\text{Mg}_{0.036}\text{Ti}_{0.011})_{\Sigma 0.999}\text{O}_3$ , which can be simplified to:  
186  $(\text{K},\text{REE},\text{Sr})(\text{Nb},\text{Cr})\text{O}_3$ . The various elements were assigned to the two cation sites (Wyckoff  
187 positions 1*b* and 1*a*, respectively) in the aristotypic perovskite formula based on size  
188 considerations and following the IMA nomenclature (Mitchell et al. 2017). A back-scattered-  
189 electron image of goldschmidtite is shown in Figure 3.

190

191

## 192 **Crystal structure**

193         The method of eight-position centering on a Huber four-circle diffractometer was used to  
194 center 46 reflections from  $\pm 30^\circ 2\theta$ , resulting in 368 total rocking curves. The diffraction spots  
195 can be described as very sharp, with a full-width at half-maximum averaging  $0.07^\circ$  in the final  
196 omega scan. Unconstrained least-squares fitting to all 46 reflections gives unit-cell parameters:  $a$   
197  $= 3.98757(20) \text{ \AA}$ ,  $b = 3.98751(22) \text{ \AA}$ ,  $c = 3.98756(20) \text{ \AA}$ ,  $\alpha = 89.999(4)^\circ$ ,  $\beta = 89.997(4)^\circ$ , and  $\gamma =$   
198  $89.999(4)^\circ$ , indicating that goldschmidtite is cubic. Cubic-constrained least squares refinement  
199 gives  $a = 3.98755(12) \text{ \AA}$  and  $V = 63.404(6) \text{ \AA}^3$ .

200         Single-crystal intensity data were collected in the range of  $-15$  to  $+60$  degrees  $2\theta$ ,  
201 resulting in 753 total reflections in a sphere of reciprocal space from  $\pm 5 h$ ,  $\pm 5 k$  and  $\pm 5 l$ , of  
202 which 33 are unique with a merging R-factor ( $R_{\text{int}}$ ) of 0.0636. From the intensity data, the space  
203 group was determined to be  $Pm\text{-}3m$  (No. 221 in the International Tables for Crystallography),  
204 being the only space group with zero observed symmetry violations. Although all atoms are on  
205 special positions in  $Pm\text{-}3m$  (Figure 4), a refinement was carried out to produce anisotropic  
206 displacement parameters and a list of reflections and structure factors provided in the  
207 crystallographic information file (CIF), yielding a final R-factor of 0.0181. In addition, the  
208 powder diffraction pattern was calculated using PowderCell version 2.4 for Windows (Kraus and  
209 Nolze 1996) for  $\text{Cu } K\alpha_1$ ,  $1.540598 \text{ \AA}$ , and is presented in Table 2. The atom assignments for the  
210 powder diffraction calculation were: Wyckoff  $1b - (\text{K}_{0.504}\text{La}_{0.15}\text{Sr}_{0.133}\text{Ba}_{0.092}\text{Ce}_{0.078})_{\Sigma 0.957}$ ;  
211 Wyckoff  $1a (\text{Nb}_{0.695}\text{Cr}_{0.201}\text{Fe}_{0.051}\text{Mg}_{0.038}\text{Al}_{0.014}\text{Ti}_{0.011})_{\Sigma 0.999}$ ; Wyckoff  $3d - \text{O}$ . Figure 5 shows an  
212 unfiltered X-ray diffraction image taken with a MAR345 image plate, demonstrating sharp  
213 diffraction spots and the absence of twinning. Goldschmidtite is most similar to isolueshite,

214 (Na,La,Ca)(Nb,Ti)O<sub>3</sub> (Krivovichev et al. 2000), which has the identical space group and similar  
215 cell dimensions (in the range 3.90-3.91 Å).

216 Although synthetic KNbO<sub>3</sub> is orthorhombic at room temperature, goldschmidtite is cubic.  
217 This may be a result of the cation occupancies: the A-site is only 50% filled by K and the B-site  
218 is 70% filled by Nb atoms. The balance is filled by smaller-sized cations (e.g., La on the A-site,  
219 Cr on the B-site), which results in goldschmidtite adopting a cubic structure as shown for the  
220 analogous synthetic system by Kakimoto et al. (2003).

221

## 222 **Raman spectrum**

223 Goldschmidtite possesses cubic symmetry, space group *Pm-3m*, with A site (K, REE, Sr), B  
224 site (Nb, Cr), and O all lying on inversion centers with site symmetry *O<sub>h</sub>*, *O<sub>h</sub>*, and *D<sub>4h</sub>*,  
225 respectively. Consequently, by selection rules, there are no Raman-active modes. As shown in  
226 Figure 6A, the as-measured (uncorrected) Raman spectrum of goldschmidtite exhibits many  
227 weak, broad bands from 100-700 cm<sup>-1</sup> and a large peak at ~815 cm<sup>-1</sup>, similar to a spectrum of  
228 natural perovskite in the RRUFF database (sample R050456) from Magnet Cove, Arkansas,  
229 USA, with composition (Ca<sub>0.82</sub>Fe<sub>0.09</sub>Na<sub>0.07</sub>Ce<sub>0.01</sub>La<sub>0.01</sub>)(Ti<sub>0.95</sub>Nb<sub>0.05</sub>)O<sub>3</sub>. In CaTiO<sub>3</sub> solid solutions  
230 with Sr(Mg,Nb)O<sub>3</sub> and NdAlO<sub>3</sub>, a strong, broad Raman band at ~820 cm<sup>-1</sup> has been attributed to  
231 partial and local ordering of multiple cations on the B site (Zheng et al. 2003; Zheng et al. 2004),  
232 suggesting that the 815 cm<sup>-1</sup> band in goldschmidtite and some CaTiO<sub>3</sub> perovskites results from  
233 non-random B-site ordering, characteristic of complex perovskites. The broad nature of the  
234 815 cm<sup>-1</sup> band in goldschmidtite suggests that ordering is short range and weak, which would  
235 therefore not be detectable in the single-crystal X-ray diffraction data.

236 In Figure 6A, the Raman spectrum of goldschmidtite is also compared with natural tausonite  
237 from the type locality and synthetic, cubic SrTiO<sub>3</sub> from the RRUFF database (sample X090004).  
238 Since SrTiO<sub>3</sub> also has the *Pm-3m* space group, no first-order Raman is expected and the  
239 observed bands are second-order features (Schaufele and Weber 1967; Nilsen and Skinner 1968).  
240 Second-order Stokes Raman scattering involves the addition or difference combination of  
241 phonons from different longitudinal-optical (LO), transverse-optical (TO), or transverse-acoustic  
242 (TA) modes (Nilsen and Skinner 1968). In Table 3, the second-order Raman band positions and  
243 assignments in SrTiO<sub>3</sub> from Nilsen and Skinner (1968) are listed along with the observed bands  
244 in goldschmidtite from a deconvolution of the baseline-corrected spectrum, shown in Figure 6B.  
245 Thus, most of the features in the measured Raman spectrum of goldschmidtite are either  
246 attributed to weak, local cation ordering or second-order Raman scattering.  
247

248

## IMPLICATIONS

249 Potassium and niobium are not common elements in the typical suite of mantle-derived  
250 minerals included in diamonds but indicate mantle metasomatism (Erlank and Rickard 1977;  
251 Dawson 1982). Several Nb-rich minerals were found in the heavy mineral concentrate from  
252 Jagersfontein and from a metasomatic vein in a peridotite from Bultfontein (both kimberlite  
253 pipes are in close proximity and age to the Koffiefontein pipe): Nb-rich perovskite (21-28 wt%  
254 Nb<sub>2</sub>O<sub>5</sub>), Nb-rich rutile (~13 wt% Nb<sub>2</sub>O<sub>5</sub>), Nb-rich titanite (11.9 wt% Nb<sub>2</sub>O<sub>5</sub>); and were believed  
255 form by the interaction of metasomatic fluids with peridotite at 20 to 30 kbar and 900 to 1000 °C  
256 (Haggerty et al. 1983). The existence of goldschmidtite indicates that perovskite-structure oxides  
257 have the potential to be significant hosts for K and Nb in the mantle, along with other lithophile  
258 elements such as La and Ce, and high-field-strength elements such as Ti and Ta. However, the  
259 precipitation of a mineral with such high concentrations of LILE (K, Ba) and strongly  
260 incompatible HFSE (Sr, LREE, Nb) requires an extremely fractionated metasomatic fluid that is  
261 much more enriched in incompatible elements than has been observed for “normal” mantle  
262 metasomatism (Hoffman 1988, Allègre et al. 1995). To stabilize such a phase would require that  
263 these incompatible elements become major components in the fractionating fluid. Thus, this  
264 would likely result from the last drops of an initially much larger volume of metasomatic melt or  
265 fluid.

266 The presence of edgarite, FeNb<sub>3</sub>S<sub>6</sub>, in an unusually reduced fenite (Barkov et al. 2000) has  
267 been interpreted recently to indicate that niobium may occur in the trivalent or tetravalent states  
268 in the mantle (Bindi and Martin 2018). However, the occurrence of goldschmidtite in diamond  
269 suggests that niobium is more likely in the pentavalent state in the mantle, at least in diamond-  
270 forming environments.

271

## ACKNOWLEDGEMENTS

272 The authors thank T. Stachel and D.G. Pearson for their comments and suggestions, which  
273 improved the quality of the manuscript. This research was supported in part by the National  
274 Research Foundation of South Africa, grant 94626 (N.A. Meyer) and a Natural Sciences and  
275 Engineering Research Council (NSERC) Discovery Grant (T. Stachel). S.D. Jacobsen  
276 acknowledges support from US National Science Foundation, grant EAR-1853521. JWH thanks  
277 the Diamond Trading Company (a member of the DeBeers Group of Companies) for the  
278 donation of the diamond used in this study.

279

280

## REFERENCES CITED

- 281 Allègre, C.J., Poirier, J., Humler, E., and Hofmann, A.W. (1995) The chemical composition of  
282 the Earth. *Earth and Planetary Science Letters*, 134, 515–526.
- 283 Angel, R.J. and Finger, L.W. (2011) SINGLE: a program to control single-crystal  
284 diffractometers. *Journal of Applied Crystallography*, 44, 247–251.
- 285 Armstrong, J.T. (1995) CITZAF: A package of correction programs for the quantitative electron  
286 microbeam X-ray-analysis of thick polished materials, thin-films, and particles. *Microbeam*  
287 *Analysis*, 4, 177–200.
- 288 Barkov, A.Y., Martin, R.F., Men'shikov, Y.P., Savchenko, Y.E., Thibault, Y., and Laajoki,  
289 K.V.O. (2000) Edgarite, FeNb<sub>3</sub>S<sub>6</sub>, first natural niobium-rich sulfide from the Khibina  
290 alkaline complex, Russian Far North: evidence for chalcophile behavior of Nb in a fenite.  
291 *Contributions to Mineralogy and Petrology*, 138, 229–236.
- 292 Barth, T. (1925) Die Kristallstruktur von Perowskit und Verwandten Verbindungen. *Norsk*  
293 *Geologisk Tidsskrift*, 8, 201–216 (in German).
- 294 Bastiansen, O.C.A. (1962) Victor Moritz Goldschmidt 1888–1947. In P.P. Ewald, Ed., *Fifty*  
295 *Years of X-Ray Diffraction*, pp. 364–365. Springer, Boston, MA.
- 296 Bindi, L., and Martin, R.F. (2018) Edgarite, FeNb<sub>3</sub>S<sub>6</sub>, from the Khibina alkaline complex,  
297 Russia: solution of the crystal structure. *Canadian Mineralogist*, 56, 259–264.
- 298 Chakhmouradian, A., Yakovenchuk, V., Mitchell, R.H., and Bogdanova, A. (1997) Isolueshite: a  
299 new mineral of the perovskite group from the Khibina alkaline complex. *European Journal of*  
300 *Mineralogy*, 9, 483–490.
- 301 Chantler, C.T., Olsen, K., Dragoset, R.A., Chang, J., Kishore, A.R., Kotochigova, S.A. and  
302 Zucker, D.S. (2005) X-ray form factor, attenuation and scattering tables, NIST Standard

- 303 Reference Database 66 (version 2.1). [Online] Available: <http://physics.nist.gov/ffast> [2018,  
304 August 22]. National Institute of Standards and Technology, Gaithersburg, MD.
- 305 Clement, C.R. (1982) A comparative geological study of some major kimberlite pipes in the  
306 Northern Cape and Orange Free State. Doctoral dissertation, University of Cape Town.
- 307 Davis, G.L. (1978) Zircons from the mantle. Short papers of the Fourth International Conference,  
308 Geochronology, Cosmochronology, Isotope Geology. Geological Survey Open-File Report,  
309 78, 86–88.
- 310 Dawson, J.B. (1982) Contrasting types of mantle metasomatism. In International Kimberlite  
311 Conference: Extended Abstracts, Vol. 3, 232–233.
- 312 Donovan, J.J., Kremser, D., Fournelle, J.H., and Goemann, K. (2015) Probe for EPMA:  
313 Acquisition, automation and analysis, version 11: Eugene, Oregon, Probe Software, Inc.
- 314 Donovan, J.J., Lowers, H.A., and Rusk, B.G. (2011) Improved electron probe microanalysis of  
315 trace elements in quartz. *American Mineralogist*, 96, 274–282.
- 316 Erlank, A.J., and Rickard, R.S. (1977) Potassic richterite bearing peridotites from kimberlite and  
317 the evidence they provide for upper mantle metasomatism. In International Kimberlite  
318 Conference: Extended Abstracts, Vol. 2, 93–95.
- 319 Field, M., Stiefenhofer, J., Robey, J., and Kurszlauskis, S. (2008) Kimberlite-hosted diamond  
320 deposits of southern Africa: A review. *Ore Geology Reviews*, 34, 33–75.
- 321 Goldschmidt, V.M. (1926) *Geochemische Verteilungsgesetze Der Elemente VII. Die Gesetze der*  
322 *Krystallochemie nach Untersuchungen gemeinsam mit T. Barth, G. Lunde, W. Zacharisen.*  
323 *Skrifter utgitt av det Norske Videnskaps-Akademi i Oslo 1: Matematisk- Naturvidenskapelig*  
324 *Klasse, 1–117 (in German).*



- 325 Gurney, J.J., Harris, J.W., and Rickard, R.S. (1984) Silicate and oxide inclusions in diamonds  
326 from the Orapa Mine, Botswana. In J. Kornprobst, Ed., *Kimberlites: II: The Mantle and*  
327 *Crust-Mantle Relationships*, 11, p. 3–9. *Developments in Petrology*, Elsevier, Amsterdam.
- 328 Gurney, J.J., Moore, R.O., Otter, M.L., Kirkley, M.B., Hops, J.J., and McCandless, T.E. (1991)  
329 Southern African kimberlites and their xenoliths. In: A.B. Kampunza and R.T. Lubala (Eds.),  
330 *Magmatism in Extensional Structural Settings*, pp. 495–536. Springer.
- 331 Haggerty, S.E. (1983) The mineral chemistry of new titanates from the Jagersfontein kimberlite,  
332 South Africa: implications for metasomatism in the upper mantle. *Geochimica et*  
333 *Cosmochimica Acta*, 47, 1833–1854.
- 334 Harris, J.W., and Gurney, J.J. (1979) Inclusions in Diamond. In J.E. Field, Ed., *The Properties of*  
335 *Diamond*, pp. 555–591. Academic Press London, London.
- 336 Harte, B., Harris, J.W., Hutchison, M.T., Watt, G.R., and Wilding, M.C. (1999). Lower mantle  
337 mineral associations in diamonds from Sao Luiz, Brazil. In Y. Fei, C.M. Bertka, and B.O.  
338 Mysen, Eds., *Mantle Petrology: Field Observations and High-Pressure Experimentation: A*  
339 *Tribute to Francis R. (Joe) Boyd*. *Geochemical Society Special Publication* 6, 125–153.
- 340 Helmstaedt, H.H., Gurney, J.J., and Richardson, S.H. (2010) Ages of cratonic diamond and  
341 lithosphere evolution: Constraints on Precambrian tectonics and diamond exploration.  
342 *Canadian Mineralogist*, 48, 1385–1408.
- 343 Hobbs, W.H. (1899) Goldschmidtite, a new mineral. *American Journal of Science*, 357–364.
- 344 Hofmann, A.W. (1988) Chemical differentiation of the Earth: the relationship between mantle,  
345 continental crust, and oceanic crust. *Earth and Planetary Science Letters*, 90, 297–314.
- 346 Holmquist, P.J. (1896) *Synthetische Studien über die Perowskit- und Pyrochlormineralien*.  
347 *Bulletin of the Geological Institution of the University of Upsala*, 3, 181–268 (in German).

- 348 Joly, A. (1877) Recherches sur les composés du niobium et du tantale. Annales Scientifiques de  
349 L'École Normal Supérieure, 6, 125–186 (in French).
- 350 Kakimoto, K.-I., Masuda, I., and Ohsato, H. (2003) Ferroelectric and piezoelectric properties of  
351 KNbO<sub>3</sub> ceramics containing small amounts of LaFeO<sub>3</sub>. Japanese Journal of Applied Physics,  
352 42, 6102–6105.
- 353 Kauffman, G.B. (1997) Victor Moritz Goldschmidt (1888–1947): A tribute to the founder of  
354 modern geochemistry on the fiftieth anniversary of his death. The Chemical Educator, 2, 1–  
355 26.
- 356 King, H.E. and Finger, L.W. (1979) Diffracted beam crystal centering and its application to high-  
357 pressure crystallography. Journal of Applied Crystallography, 12, 374–378.
- 358 Kiseeva, E.S., Wood, B.J., Ghosh, S., and Stachel, T. (2016) The pyroxenite-diamond  
359 connection. Geochemical Perspectives Letters, 2, 1–9.
- 360 Kopylova, M.G., Gurney, J.J., and Daniels, L.R.M. (1997) Mineral inclusions in diamonds from  
361 the River Ranch kimberlite, Zimbabwe. Contributions to Mineralogy and Petrology, 129,  
362 366–384.
- 363 Kraus, W., and Nolze, G. (1996) POWDER CELL - a program for the representation and  
364 manipulation of crystal structures and calculation of the resulting X-ray powder patterns.  
365 Journal of Applied Crystallography, 29, 301–303.
- 366 Laves, F. (1962) The growing field of mineral structures. In P.P. Ewald, Ed., Fifty Years of X-  
367 Ray Diffraction, pp. 174–189. Springer, Boston, MA.
- 368 Lummen, T.T.A., Leung, J., Kumar, A., Wu, X., Ren, Y., VanLeeuwen, B.K., Haislmaier, R.C.,  
369 Holt, M., Lai, K., Kalinin, S.V., and Gopalan, V. (2017) Emergent low-symmetry phases and

- 370 large property enhancements in ferroelectric KNbO<sub>3</sub> bulk crystals. *Advanced Materials*, 29,  
371 1700530, 1–7.
- 372 Mandarino, J.A. (1976) The Gladstone-Dale relationship - Part I: Derivation of new constants.  
373 *Canadian Mineralogist*, 14, 498–502.
- 374 Mason, B.H. (1992) Victor Moritz Goldschmidt: Father of Modern Geochemistry, 184 p.  
375 Geochemical Society, Special Publication No. 4, San Antonio.
- 376 Meyer, H.O.A. (1987) Inclusions in diamond. In P.H. Nixon, Ed., *Mantle Xenoliths*, pp. 501–  
377 522. John Wiley and Sons.
- 378 Mitchell, R.H., Choi, J.B., Hawthorne, F.C., and Burns, P.C. (1998) Latrappite: A re-  
379 investigation. *Canadian Mineralogist*, 36, 107–116.
- 380 Mitchell, R.H., Welch, M.D., and Chakhmouradian, A.R. (2017) Nomenclature of the perovskite  
381 supergroup: A hierarchical system of classification based on crystal structure and  
382 composition. *Mineralogical Magazine*, 81, 411–461.
- 383 Naidoo, P., Stiefenhofer, J., Field, M., and Dobbe, R. (2004) Recent advances in the geology of  
384 Koffiefontein Mine, Free State Province, South Africa. *Lithos*, 76, 161–182.
- 385 Nestola, F., Korolev, N., Kopylova, M., Rotiroti, N., Pearson, D.G., Pamato, M.G., Alvaro, M.,  
386 Peruzzo, L., Gurney, J.J., Moore, A.E., and Davidson, J. (2018) CaSiO<sub>3</sub> perovskite in  
387 diamond indicates the recycling of oceanic crust into the lower mantle. *Nature*, 555, 237–  
388 241.
- 389 Nilsen, W.G., and Skinner, J.G. (1968) Raman spectrum of strontium titanate. *Journal of*  
390 *Chemical Physics*, 48, 2240–2248.

- 391 Nimis, P., and Taylor, W.R. (2000) Single clinopyroxene thermobarometry for garnet peridotites.  
392 Part I. Calibration and testing of a Cr-in-Cpx barometer and an enstatite-in-Cpx thermometer.  
393 Contributions to Mineralogy and Petrology, 139, 541–554.
- 394 Palache, C. (1900) Notes on tellurides from Colorado. American Journal of Science, 419–427.
- 395 Palot, M., Jacobsen, S.D., Townsend, J.P., Nestola, F., Marquardt, K., Miyajima, N., Harris,  
396 J.W., Stachel, T., McCammon, C.A., and Pearson, D.G. (2016) Evidence for H<sub>2</sub>O-bearing  
397 fluids in the lower mantle from diamond inclusion. Lithos, 265, 237–243.
- 398 Peacock, M.A. (1939) Goldschmidtine, a newly recognized antimonide of silver. American  
399 Mineralogist, 24, 227–241.
- 400 ——— (1940) Goldschmidtine identical with stephanite. American Mineralogist, 25, 372–373.
- 401 Pearson, D.G., Brenker, F.E., Nestola, F., McNeill, J., Nasdala, L., Hutchison, M.T., Matveev,  
402 S., Mather, K.A., Silversmit, G., Schmitz, S., and others (2014) Hydrous mantle transition  
403 zone indicated by ringwoodite included within diamond. Nature, 507, 221–4.
- 404 Rickard, R.S., Harris, J.W., Gurney, J.J., and Cardoso, P., (1989) Mineral inclusions in diamonds  
405 from Koffiefontein Mine. In Kimberlites and Related Rocks, 2, 1054–1062.
- 406 Schaufele, R.F., and Weber, M.J. (1967) First- and second-order Raman scattering of SrTiO<sub>3</sub>.  
407 The Journal of Chemical Physics, 46, 2859–2861.
- 408 Skjærvø, S.L., Høydalsvik, K., Blichfeld, A.B., Einarsrud, M.-A., and Grande, T. (2018)  
409 Thermal evolution of the crystal structure and phase transitions of KNbO<sub>3</sub>. Royal Society  
410 Open Science, 5, 180368, 1–5.
- 411 Suess, H.E. (1988) V.M Goldschmidt and the origin of the elements. Applied Geochemistry, 3,  
412 385–391.

- 413 Tilley, C.E. (1948) Victor Moritz Goldschmidt. Biographical Memoirs of Fellows of the Royal  
414 Society, 6, 51–66.
- 415 Tschauner, O., Ma, C., Beckett, J.R., Prescher, C., Prakapenka, V.B., and Rossman, G.R. (2014)  
416 Discovery of bridgmanite, the most abundant mineral in Earth, in a shocked meteorite.  
417 Science, 346, 1100–1102.
- 418 Tschauner, O., Huang, S., Greenberg, E., Prakapenka, V.B., Ma, C., Rossman, G.R., Shen, A.H.,  
419 Zhang, D., Newville, M., Lanzirrotti, A., and others (2018) Ice-VII inclusions in diamonds:  
420 Evidence for aqueous fluid in Earth’s deep mantle. Science, 359, 1136–1139.
- 421 Zheng, H., Csete de Györgyfalva, G.D.C., Quimby, R., Bagshaw, H., Ubic, R., Reaney, I.M., and  
422 Yarwood, J. (2003) Raman spectroscopy of B-site order-disorder in CaTiO<sub>3</sub>-based  
423 microwave ceramics. Journal of the European Ceramic Society, 23, 2653–2659.
- 424 Zheng, H., Reaney, I.M., and Gyo, G.D.C.C. De (2004) Raman spectroscopy of CaTiO<sub>3</sub>-based  
425 perovskite.
- 426

**LIST OF FIGURE CAPTIONS**

427

428

429 **FIGURE 1.** Broken and rounded dodecahedral diamond from Koffiefontein that hosted  
430 goldschmidtite (before breakage). Goldschmidtite is seen in green and radiation damage of  
431 the diamond can be seen by the brown regions.

432 **FIGURE 2.** Two orientations of the crystal of goldschmidtite adhered to a glass fiber. Crystal  
433 shape has been affected by polishing. Background noise due to the digital-image stacking has  
434 been removed.

435 **FIGURE 3.** Back-scattered-electron image of goldschmidtite. The lamellar structure is probably a  
436 result of polishing.

437 **FIGURE 4.** Clinographic view of the structure of goldschmidtite: Nb atoms are orange and in 6-  
438 fold coordination, K is pale blue and in 12-fold coordination, O atoms are red, and the unit  
439 cell is shown in black.

440 **FIGURE 5.** X-ray diffraction image (Mo  $K\alpha$  radiation) taken with a MAR345 image plate  
441 showing sharp, single diffraction spots and the absence of twinning.

442 **FIGURE 6. (a)** Uncorrected Raman spectrum of goldschmidtite (black) using a 458.5 nm  
443 excitation laser, compared with natural tausonite (red curve) and perovskite (blue curve,  
444 RRUFF sample R050456). Spectra are offset for clarity. Raman features in SrTiO<sub>3</sub> are  
445 attributed to second-order Raman scattering (Nilsen and Skinner 1968). The strong band at  
446 815 cm<sup>-1</sup> is likely due to weak, local ordering of different cations on the B site (Zheng et al.  
447 2003). **(b)** Deconvolved and baseline-corrected Raman spectrum of goldschmidtite below  
448 1200 cm<sup>-1</sup>.

449

450 **TABLE 1.** Electron microprobe analysis of goldschmidtite.

<b>Constituent</b>	<b>wt%</b>	<b>Range (n=11)</b>	<b>Stand. dev.</b>
Nb <sub>2</sub> O <sub>5</sub>	44.82	43.97 – 46.04	0.69
TiO <sub>2</sub>	0.44	0.42 – 0.46	0.01
ThO <sub>2</sub>	0.1	0 – 0.16	0.06
Al <sub>2</sub> O <sub>3</sub>	0.35	0.32 – 0.39	0.02
Cr <sub>2</sub> O <sub>3</sub>	7.07	6.80 – 7.15	0.11
La <sub>2</sub> O <sub>3</sub>	11.85	11.45 – 12.05	0.17
Ce <sub>2</sub> O <sub>3</sub>	6.18	6.02 – 6.29	0.08
Fe <sub>2</sub> O <sub>3</sub>	1.96	1.95 – 1.98	0.01
MgO	0.7	0.67 – 0.78	0.03
CaO	0.04	0.02 – 0.07	0.01
SrO	6.67	6.14 – 6.83	0.21
BaO	6.82	6.48 – 7.30	0.27
K <sub>2</sub> O	11.53	11.16 – 11.67	0.14
Total	98.53	97.81 – 99.81	0.58

451

452

453 **TABLE 2.** Calculated powder diffraction data for goldschmidtite.

<i>Relative intensity, I (%)</i>	<i>d<sub>calc.</sub> (Å)</i>	<i>hkl</i>
0.61	3.9876	100
100.00	2.8197	110
6.89	2.3022	111
49.93	1.9938	200
0.22	1.7833	210
57.80	1.6279	211
35.82	1.4098	220
0.01	1.3292	300
0.05	1.3292	221
28.15	1.2610	310
2.11	1.2023	311
12.89	1.1511	222
0.02	1.1060	320
37.95	1.0657	321
7.30	0.9969	400
0.02	0.9671	410
0.02	0.9671	322
8.63	0.9399	330
17.25	0.9399	411
1.13	0.9148	331
29.88	0.8917	420
0.03	0.8702	421
20.86	0.8502	332
43.24	0.8140	422

454

455

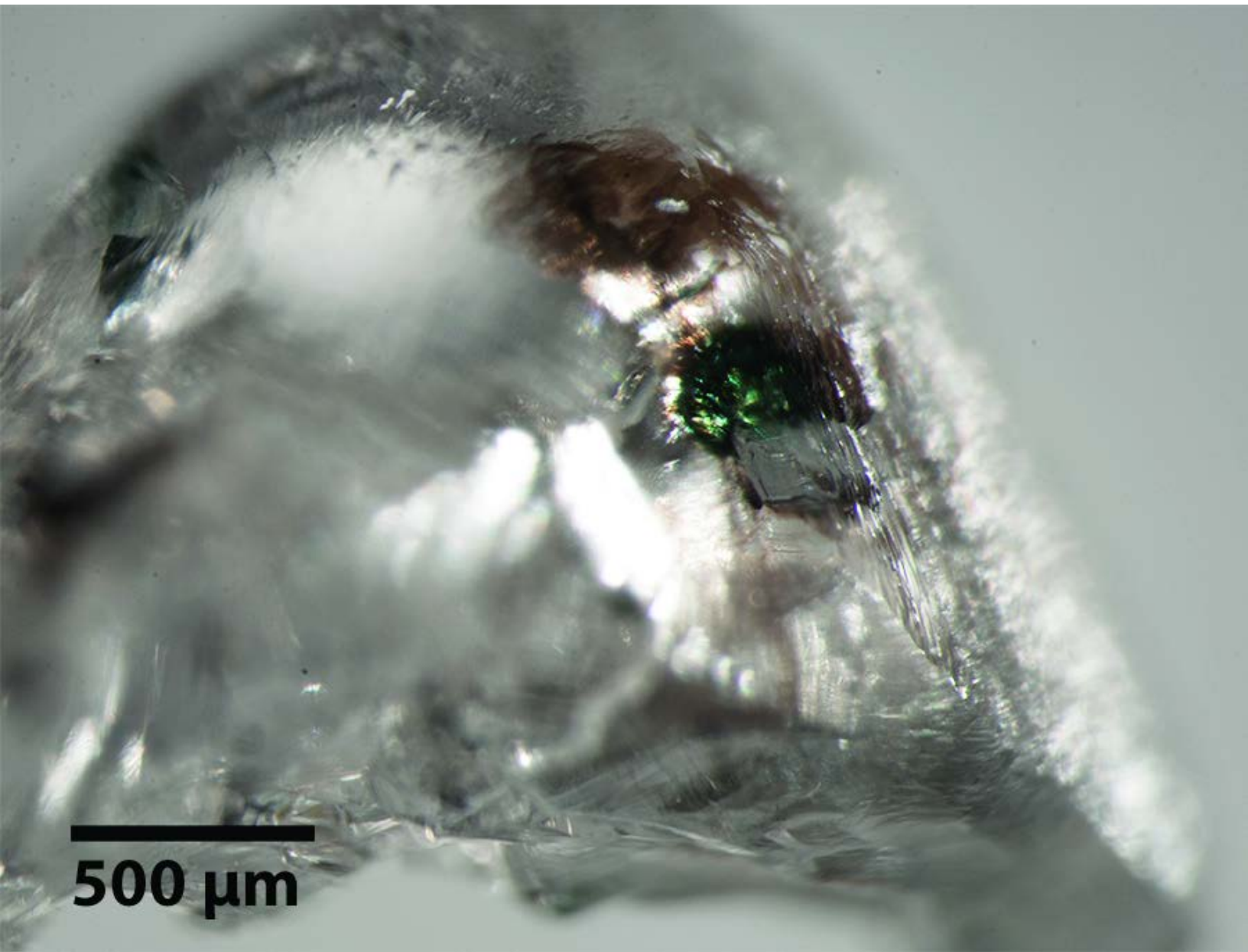


456 **TABLE 3.** Raman spectral assignments for second-order modes.

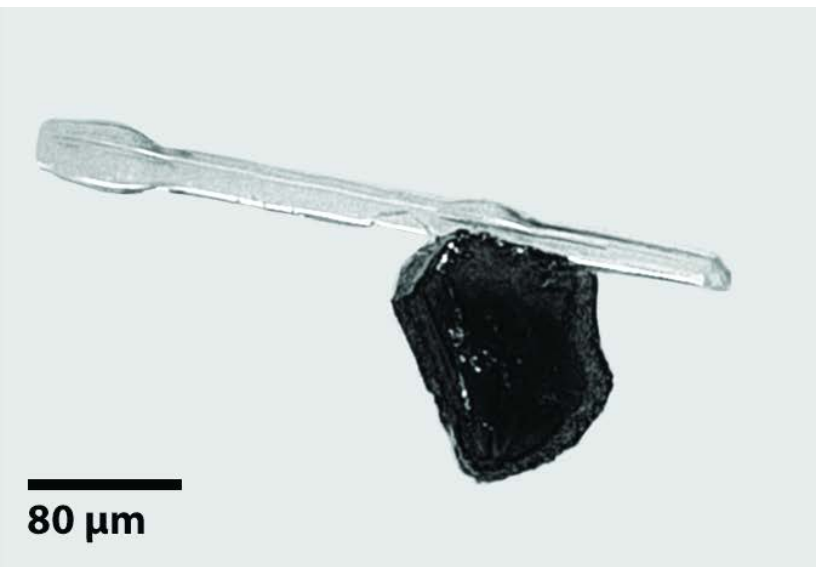
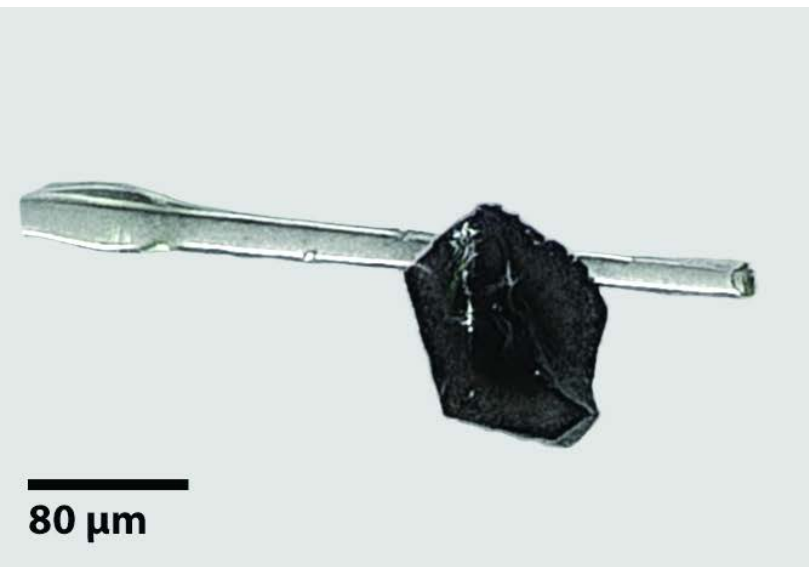
Goldschmidtite (cm <sup>-1</sup> )	SrTiO <sub>3</sub> (cm <sup>-1</sup> ) <sup>a</sup>	Assignments for SrTiO <sub>3</sub> <sup>a</sup>
125	81	TO <sub>2</sub> -TA; TO <sub>2</sub> -TO <sub>1</sub>
160		
240	251	2TA; 2TO <sub>1</sub> ; TO <sub>1</sub> +TA
320	308	TO <sub>2</sub> +TA; TO <sub>2</sub> +TO <sub>1</sub> ; TO <sub>4</sub> - TO <sub>2</sub>
	369	TO <sub>4</sub> -TA; TO <sub>4</sub> -TO <sub>1</sub> ; 2TO <sub>2</sub>
445		
465		
580	629	TO <sub>4</sub> +TA; TO <sub>4</sub> +TO <sub>1</sub>
	684	2TO <sub>3</sub>
715	727	TO <sub>4</sub> +TO <sub>2</sub>
750		
815		
850	1038	2LO <sub>2</sub> ; 2TO <sub>4</sub>
	1325	LO <sub>4</sub> +LO <sub>2</sub>
1590	1618	2LO <sub>4</sub>

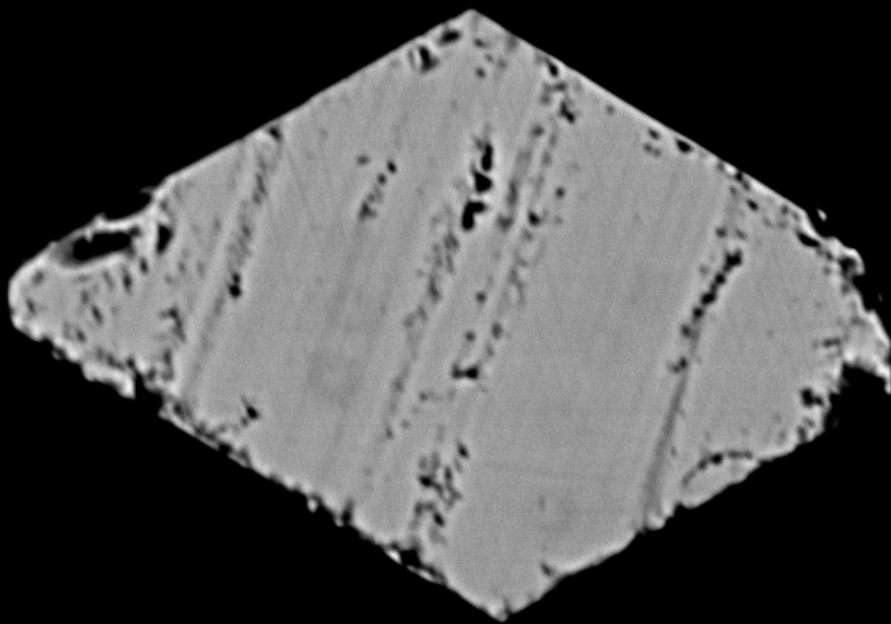
457 <sup>a</sup> Synthetic, pure SrTiO<sub>3</sub> (Nilsen and Skinner 1968).

458



500 μm





147

129

110

92

74

55

37

18

0

50.  $\mu\text{m}$  ESE 20. kV

